

See discussions, stats, and author profiles for this publication at: <https://www.researchgate.net/publication/256836040>

A Mechanism for the Uncatalyzed Cyclic Acetone-Peroxide Formation Reaction: An Experimental and Computational Study.

ARTICLE in THE JOURNAL OF PHYSICAL CHEMISTRY A · SEPTEMBER 2013

Impact Factor: 2.69 · DOI: 10.1021/jp406972k · Source: PubMed

READS

76

6 AUTHORS, INCLUDING:



[Leonardo C Pacheco-Londono](#)

University of Puerto Rico at Mayagüez

83 PUBLICATIONS 502 CITATIONS

[SEE PROFILE](#)



[Ricardo Vivas-Reyes](#)

Universidad de Cartagena

58 PUBLICATIONS 327 CITATIONS

[SEE PROFILE](#)



[Samuel P Hernández-Rivera](#)

University of Puerto Rico at Mayagüez

210 PUBLICATIONS 960 CITATIONS

[SEE PROFILE](#)

Mechanism for the Uncatalyzed Cyclic Acetone-Peroxide Formation Reaction: An Experimental and Computational Study

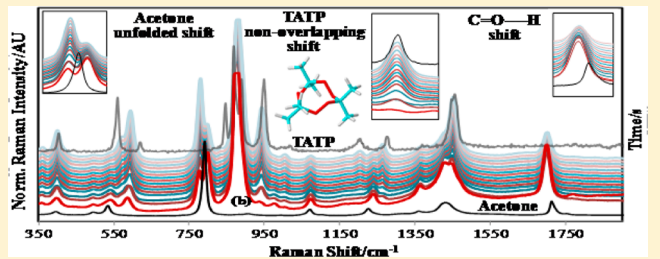
Eduardo A. Espinosa-Fuentes,[†] Leonardo C. Pacheco-Londoño,[†] Migdalia Hidalgo-Santiago,[†] Martha Moreno,[‡] Ricardo Vivas-Reyes,^{*,‡} and Samuel P. Hernández-Rivera[†]

[†]Center for Chemical Sensors Development/Chemical Imaging Center ALERT DHS-Center of Excellence for Explosives Detection, Mitigation and Response, Department of Chemistry, University of Puerto Rico-Mayaguez, PO Box 9000, Mayaguez, Puerto Rico 00681-9000

[‡]Theoretical and Quantum Chemistry Group Department of Chemistry, University of Cartagena, Z/cilla-campus, Cartagena, Colombia 130015

Supporting Information

ABSTRACT: In this study, a mechanism for the uncatalyzed reaction between acetone and hydrogen peroxide is postulated. The reaction leads to the formation of the important homemade explosives collectively known as cyclic acetone peroxides (CAP). The proposed mechanistic scheme is based on Raman, GC-MS, and nuclear magnetic resonance measurements, and it is supported by *ab initio* density functional theory (DFT) calculations. The results demonstrate that the proposed mechanism for the uncatalyzed formation reaction of CAP occurs in three steps: monomer formation, polymerization of the 2-hydroperoxipropan-2-ol monomer, and cyclization. The temporal decay of the intensities of important assigned-bands is in excellent agreement with the proposed mechanism. Previous reports also confirm that the polymerization step is favored in comparison to other possible pathways.



INTRODUCTION

The reaction between acetone and hydrogen peroxide results in the formation of cyclic peroxides collectively known as cyclic acetone peroxides (CAP). One of the most famous of these compounds is the cyclotrimer or triacetone triperoxide (TATP).¹ This compound is a highly unstable explosive and has been persistently used in terrorist attacks worldwide. In addition, it was used as a detonator by the "shoe bomber", Richard Reid, in 2001.^{2–4} TATP is as powerful as ordinary military explosives, such as TNT, RDX, and PETN. However, it is one of the most sensitive explosives known with respect to initiation by impact, heat, and friction.^{5,6} Another homemade explosive (HME) based on hydrogen peroxide is hexamethylene triperoxide diamine (HMTD) which, when compared to TATP, requires more chemistry skills to prepare and is more stable and easier to handle, but is still a very powerful and dangerous highly energetic material (HEM).⁷

An important consideration in the area of HME preparations is the fact that some of them can be prepared from household or consumer products. So, their production and use is extremely difficult to control by security enforcing authorities. As a result, these agencies are highly interested in gaining more control over HME production and use. Information about reaction pathways helps improve two important security aspects. The first aspect deals with the possibility of inhibiting the formation of HME by adding interfering agents. The second aspect has to do with devising new methods of forensic analysis that may assist in

tracing energetic materials to the perpetrators. Another advantage of elucidating reaction mechanisms is that it could lead to the possibility of substituting household chemicals with passive equivalents that may inhibit the formation of HME.

The analysis and detection of TATP and other HMEs has increased in recent years. This is motivated in part by the increased use of TATP and other cyclic organic peroxides in terrorist activities.^{2–4} Many groups have studied the preparation and characterization of HME as well as possible methods to improve its detection. Recently in 2013 Oxley et al. reported a mechanistic study of the acid-catalyzed CAP-reaction at high acid concentration (≤ 2 M), in which they postulate some of the intermediate structures reported here.^{8,9} In 2008, Jensen et al. proposed a mechanism for acetone-peroxide reaction based on Raman and X-ray diffraction measurements.¹⁰ Later that year, Armitt, Zimmermann, and Ellis analyzed the degradation products of TATP using gas chromatography–mass spectrometry (GC-MS).¹¹ They found that metal ions and salts can also degrade TATP and other peroxides.

In 2007, Terent'ev et al. presented a new method to prepare 1,2,4,5,7,8-hexaoxonanes from the reaction of 1,1'-dihydroperoxydicycloalkyl peroxides with acetals and enols catalyzed by Lewis acids.¹² This method allowed the synthesis of new

Received: February 19, 2013

Revised: September 11, 2013

Published: September 19, 2013



compounds of the type described obtaining higher yields and selectivity. They found that alkoxy-peroxide reactivity is higher than acetone peroxide reactivity. In 1972, Sauer and Edwards reported higher adducts of the CAP formation reaction in acidic conditions, which are precursors of the cyclotrimer and cyclotetramer. In 1971 they reported that AP reaction produces 2-hydroxy-2-hydroperoxy propane and they determined the thermodynamic constants.^{13,14} In 1970, Story et al. proposed a mechanism of the acid-catalyzed AP reaction, in which they proposed that cyclotrimer is the kinetic product of this type of reaction.¹⁵

The goal of this research was to propose a viable mechanism for uncatalyzed-CAP formation reaction based entirely on qualitative and quantitative Raman and NMR spectroscopy measurements and supported by DFT theoretical modeling of the proposed intermediate and transition states.

■ EXPERIMENTAL SETUP

1. Reagents. Certified ACS acetone (99.7% purity) and hydrogen peroxide (stabilized and certified, 50% aqueous solution) were obtained from Fisher Scientific International, Pittsburgh, PA. Reagents were used without further purification. Ultra high purity water (UHP, 18.2 MΩ) produced by a Nanopure system, Barnstead International, Dubuque, IA (Thermo-Fisher Scientific) was used for preparation of aqueous solutions and for washing precipitated TATP crystals after synthesis.

2. Experimental Details. Raman spectroscopy was used to monitor the reaction between acetone and peroxide. Raman spectra were collected daily to examine the reaction course. Spectral acquisitions were stopped when the first TATP crystals began to appear, which according to the literature is close to thirty days for the uncatalyzed reaction.¹ In order to carry out the daily measurements, hydrogen peroxide and acetone were mixed in 1:1 molar ratio in clear glass vials at room temperature (~22 °C). Kinetic runs of the reaction mixtures were temporally recorded using Raman spectroscopy in the temperature range from 30 to 60 °C. To maintain control of the temperature a rectangular flow cell, model 72-Q-10, obtained from Starna Cells, Inc. (Atascadero, CA), was used for the experiments. All spectral measurements were obtained at 514.5 and 532 nm laser excitation lines and then compared for changes in relative intensity patterns. In order to corroborate changes in the chemical environment of the carbonyl carbon atom and methyl group as the reaction progressed, nuclear magnetic resonance measurements of the reaction mixture were obtained every two days, because the reaction rate of the uncatalyzed system is slow.¹⁶

3. Equipment and Spectral Conditions. Raman spectra were acquired using the following conditions: Raman shift range, 100–3200 cm⁻¹; accumulations, 2; acquisition time, 10 s; laser power levels, 10–60 mW; excitation lines (1) 514.5 nm laser line of a Coherent INNOVA 308, argon ion laser line; and (2) 532 nm laser line of an Excelsior-532 Spectra-Physics, solid state diode laser system. For these measurements, Renishaw RM2000 and RM1000 Raman Microspectrometers were used. For the nuclear magnetic resonance measurement experiments a Bruker FT-NMR Advance 500 MHz Spectrometer, Bruker Instruments, Inc. (Billerica, MA), was used. Typical conditions for nuclear magnetic resonance measurements were as follows. For acquisition of ¹H NMR spectra, the experimental conditions were as follows: deuterium oxide (D₂O) and acetone-*d*₆ solvents; number of transients (NS), 16; spectral width (SWH), 10330.578 Hz; and acquisition time (AQ), 3.172 s. For ¹³C NMR spectra, the

conditions were as follows: D₂O and acetone-*d*₆ solvents; NS, 32; SWH, 30030 Hz; and AQ, 1.09124.

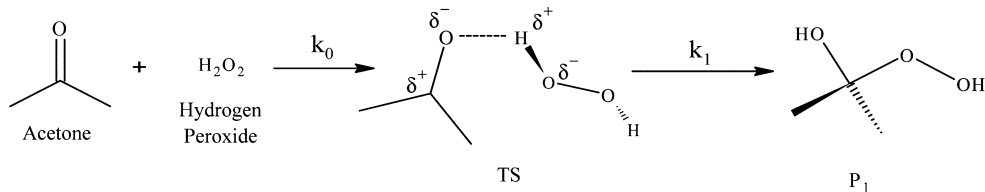
Gas chromatography analysis was performed using an Agilent GC 5890 equipped with a Supelco SPB-5 (5% biphenyl/95% dimethylsiloxane, C-18 15.0 m, 250 μm × 0.25 μm) column and coupled to a 5790 mass selective detector; the GC conditions were as follows: (I) Inlet: Temp. 150 °C; splitless mode; constant flow; (II) Oven: Initial Temp. 80 °C; Ramp 10 °C/min; final temp. 230 °C; carrier gas: He (Praxair-PR, Gurabo, PR).

4. Density Functional Theory Calculations. To carry out the theoretical calculations, first, the structures of the relevant molecules were constructed using GaussView software package, and then, the connectivity Z-matrix of the implied structures was reorganized using Molden software package taking into account the most likely interaction points. Transition state geometries (TS) were optimized followed by frequency calculations to verify that the optimized geometry used in the intrinsic reaction coordinate (IRC)¹⁷ calculation was in fact a transition state. Finally, an IRC calculation following in both directions from the ST-structure was done. The IRC calculation of the subsequent steps could not be modeled as in the first step, because it was not possible to find a transition state between two monomer molecules or this reaction occurs rapidly and has no transition state; so it was proposed considering the atomic charges densities, the second order kinetic pattern observed, and the Terent'ev et al. results.¹² The activation energy of the dimerization step was estimated scanning the reaction coordinate of the proposed interaction. This theoretical analysis was performed at the density functional theory (DFT) level using Beck's three-parameter modification¹⁸ of Lee-Yang-Parr¹⁹ hybrid functional (B3LYP) and 6-31+g(d,p)²⁰ basis set. Gaussian 03 software package²¹ was used for the calculations. Finally, properties of ground states and intermediate states of the reactions were computed, analyzed, and compared to the experimental data.

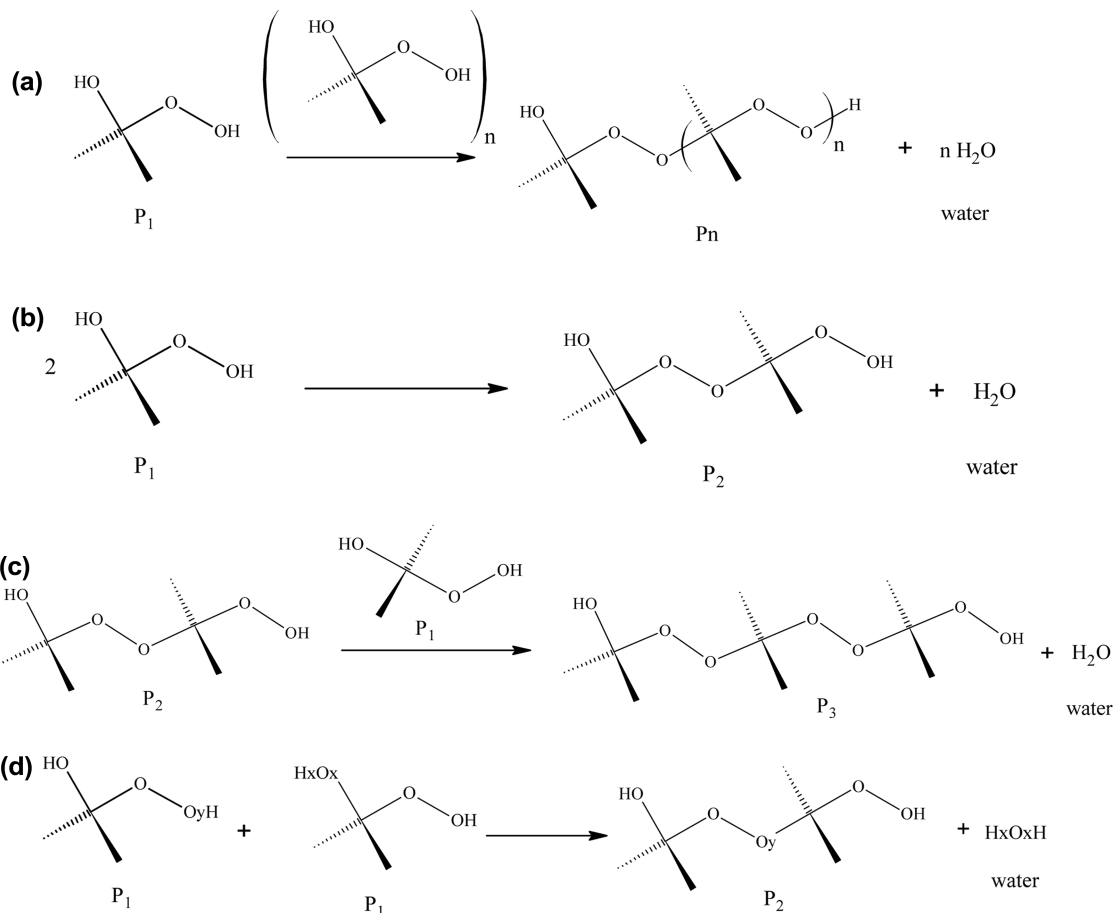
■ RESULTS AND DISCUSSION

1. Description of the CAP Formation Mechanism. The uncatalyzed acetone-peroxide formation reaction was followed for several days using Raman, NMR spectroscopies, and GC-MS, and theoretically modeled using DFT calculations to characterize the starting materials, the final products, and the possible reaction intermediates and transition states in order to propose the following mechanism, which is postulated to occur in three steps: monomer formation P₁ (2-hydroperoxy-2-propan-2-ol), polymerization, and then cyclization (see Schemes 1, 2, and 3).

At the onset of the reaction, a hydrogen peroxide molecule interacts with an acetone molecule (Scheme 1). In the polymerization and cyclization steps, the hydroperoxy and alkoxy terminal groups react by eliminating a water molecule via a condensation (HPC) reaction. Scheme 2a illustrates the process in general form, while Scheme 2b shows the process specifically for the formation of the dimer P₂ (2-[2-hydroperoxy-2-propan-2-yl] peroxy), and Scheme 2c describes the formation of P₃. The details of bonds broken and formed are depicted in the Scheme 2d. Schemes 3a and b illustrate the third and final step: cyclization by condensation. Scheme 3a illustrates the formation of the dimeric structure (C₂): diacetone diperoxide (DADP). Scheme 3b shows the cyclization of P₃ (2-[2-hydroperoxy-2-propan-2-yl] peroxy) to form the trimeric cyclic structure (C₃): triacetone triperoxide (TATP). In short, the second and third steps were proposed to occur through a hydroperoxy condensation (HPC) reaction. Other possible reactions such as the reaction between polymers structures (P_n)

Scheme 1^a

^aAcetone and hydrogen peroxide molecules start interacting at close range by forming a hydrogen bond. This process is very fast and is not included in overall mechanism proposed. Monomer formation from intermediary or transition state (TS). Monomer is designed as P_1 : (2-hydroperoxy, 2-propan-2-ol).

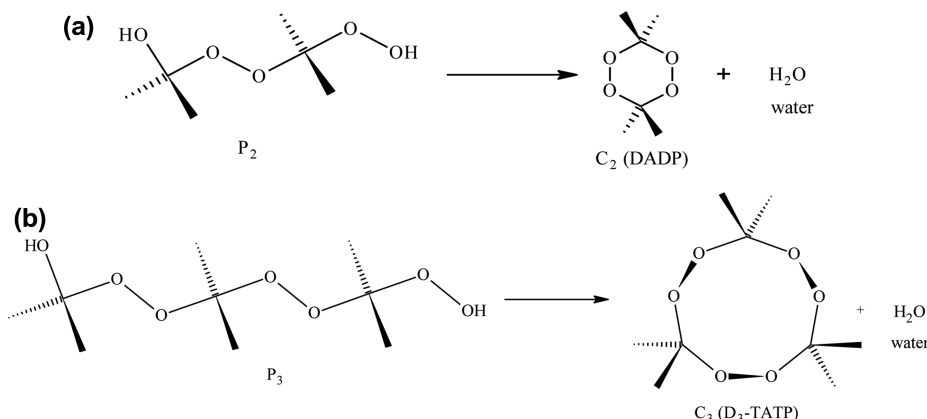
Scheme 2^a

^a(a) Second step: alkoxy-peroxy condensation reaction: general scheme for polymerization step. (b) Dimerization between two P_1 molecules and formation of P_2 dimer: $(2\text{-[2-hydroperoxy propan-2-yl] peroxy})\text{ propan-2-ol}$. (c) Formation reaction of P_3 (an alkoxy-peroxy condensation reaction) from P_2 and P_1 reacting molecules (trimmerization). Trimer is designed as P_3 ($2 \cdot \{2\text{-[2-hydroperoxy propan-2-yl] peroxy}\} \text{ propan-2-yl}$ propan-2-ol). (d) Postulation of details of polymerization step: bonds broken and formed. The proton atom can be provided by the water molecule.

of different orders were not sketched in the above schemes, but they were considered in the deduction of the total kinetic.

2. Monomer Formation Step. These two interacting molecules are already well oriented for the reaction due to the formation of hydrogen bond. In fact, the hydrogen bond readily forms when acetone is dissolved in water. This was evidenced by band broadening and red-shifting of the band assigned to the $\text{C}=\text{O}$ bond (carbonyl) in the acetone spectrum as illustrated in detail in Figure 1 for the Raman spectra for neat acetone, acetone–water solution, and acetone–hydrogen peroxide reaction mixture. A significant red-shift can be observed for both the acetone–water solution spectrum ($1640\text{--}1725\text{ cm}^{-1}$) and for the reaction mixture spectrum ($1600\text{--}1700\text{ cm}^{-1}$).

This can be contrasted to neat acetone spectrum where the range for the free carbonyl is $1700\text{--}1750\text{ cm}^{-1}$. The reaction mixture shows a larger shift of $\Delta\phi \sim -40\text{ cm}^{-1}$, indicative of a stronger interaction rather than a simple hydrogen bond. Figure 2 illustrates the change in the chemical environment of the acetone molecule as the reaction progresses as evidenced from Raman spectra. At the onset of the chemical transformation, the reaction mix and acetone Raman spectra are roughly similar, and only a minimal shift due to hydrogen bonding is observed. Then, the spectra change according to the formation of principal intermediates and cyclic product (TATP), whose splitting and characteristic bands appear specifically at 590 cm^{-1} , 800 cm^{-1} , 1450 cm^{-1} , and 960 cm^{-1} ; these vibrational bands correspond to

Scheme 3^a

^a(a) Alkoxy-peroxy cyclocondensation reaction of P_2 : formation reaction of C_2 . This cyclic acetone peroxide product is identified as 3,3,6,6-tetramethyl-1,2,4,5-cyclotetraoxane or diacetone diperoxide (DADP). (b) Alkoxy-peroxy cyclocondensation reaction of P_3 : formation reaction of C_3 . This cyclic acetone peroxide product is 3,3,6,6,9,9-hexamethyl-1,2,4,5,7,8 hexoxonane or triacetone triperoxide (TATP).

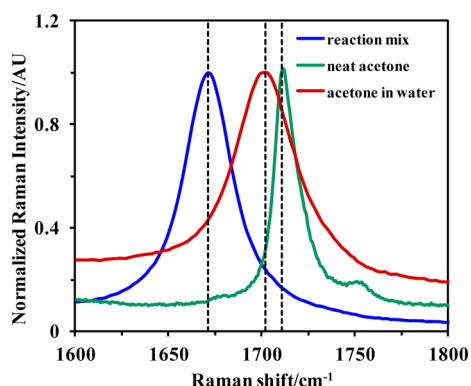


Figure 1. Variation of C=O Raman shift location due to the hydrogen bonding formation from normal range of 1690–1740 cm⁻¹ to 1600–1700 cm⁻¹.

the deformation of O-C-O angle (δ_{O-C-O}) of monomer molecule, symmetric stretching of C-C bond ($\nu_{s,C-C}$), and deformation CH₃ (δ_{CH_3}) of the acetone molecule and asymmetric stretching of C-O bond ($\nu_{a,C-O}$) of the TATP molecule, respectively, and they were assigned using the

theoretical vibrational spectra at DFT level of theory using B3LYP and 6-31+g (d,p)^{18–20} basis set.

On the other hand, carbonyl bonded to the peroxide hydrogen band ($\nu_{C=O-H(peroxy)}$), which appears at 1660 cm⁻¹ and spanned to a wavenumber range of 1600–1700 cm⁻¹ due to the formation of the hydrogen bond in acetone is surrounded by hydrogen peroxide and water molecules, and it is completely consumed in the first step. Therefore, this molecule cannot appear in the subsequent mechanism steps as shown in the reaction schemes. Consistently, the Raman intensity related to this band decayed following a first order decay rather than a more complex pattern to form the monomer molecule. These results lead to the first assumption of the proposed mechanism in which acetone is only consumed in a single reaction step (see Figure 3).

To analyze the kinetic pattern of the acetone until the appearance of the first crystals of TATP, the CAP reaction was catalyzed with sulfuric acid at low concentration (~0.05M), because the uncatalyzed reaction is too slow to obtain meaningful results. It was found that the Raman intensity of the carbonyl band ($\nu_{C=O-H}$) initially decays with a kinetic pattern of first order to form the monomer molecule, and then it is held constant during the polymerization step, and finally when the first insoluble crystals of TATP are formed by Le Chatelier-Braun

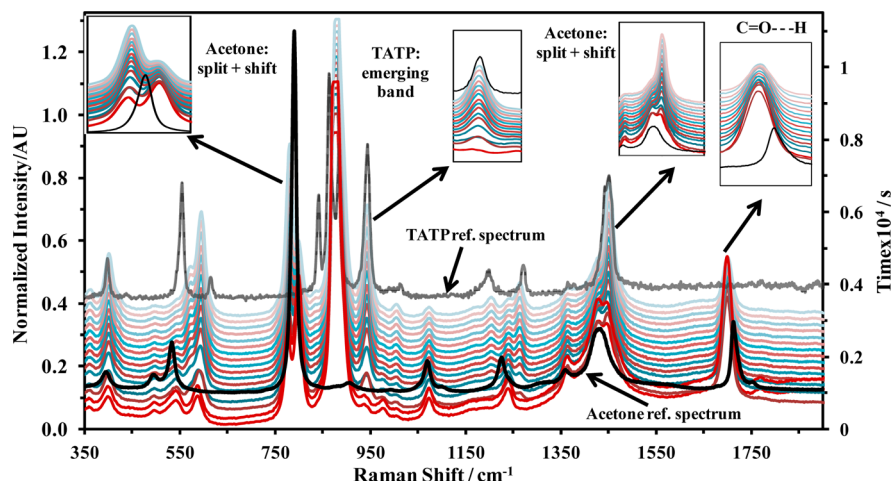


Figure 2. Variation of Raman shift band wavenumber location during a kinetic run. No significant difference between the initial spectrum and acetone spectrum was observed. Individual spectra were normalized to highest intensity peak and have been offset for clarity.

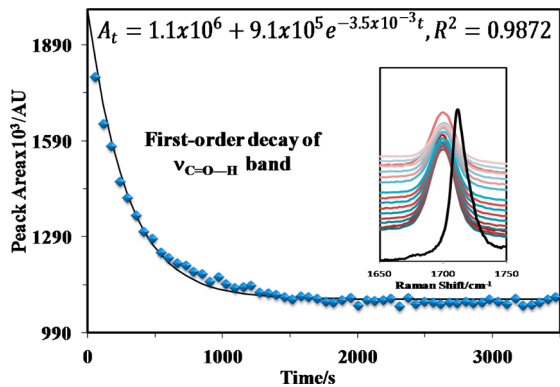


Figure 3. First-order decay of the C=O—H band intensity for an uncatalyzed reaction. The concentration of the AP complex does not decay completely to zero; this effect was explained with AP-catalyzed reaction.

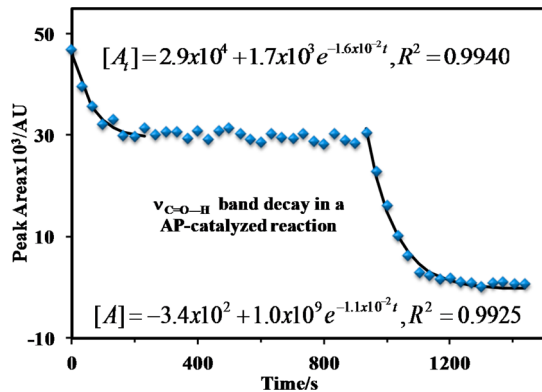


Figure 4. Intensity decay of $\nu_{\text{C=O}}$ band during a kinetics run of a catalyzed AP-reaction.

principle, it follows consuming with a first order decay as is shown in Figure 4. The final decay was related to Le Chatelier–Braun principle, because the rate constants of the final decay for several bands have the same value. Again, this leads to the first assumption of the mechanism proposed: acetone is consumed in a single reaction step. The same happens with other new bands are formed in the spectral range of 532–620 cm⁻¹ (see Figure 5).

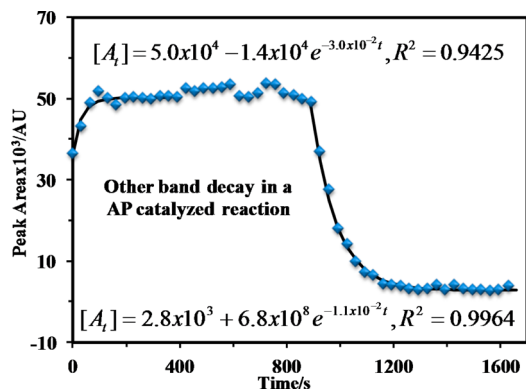


Figure 5. Intensity decay of other bands during a kinetics run of a catalyzed AP-reaction.

3. Theoretical Support of the Monomer Formation Step.

According to intrinsic reaction coordinate (IRC) theoretical results, the transition state of the first step is

postulated to proceed via formation of hydrogen bonding between the interacting molecules, in which the hydrogen atom gets closer to the oxygen atom to form the O—H bond and carbonyl bond decreases its bond order from 2 to 1.5, by changing from a triangular planar structure to a nearly tetrahedral structure. The diminished electron density on the carbonyl C atom is then concertedly attacked by the peroxide oxygen atom as illustrated in Figure 6. The bond length for a normal H—O bond in an optimized hydrogen peroxide structure is 0.96 Å. The O—H bond lengths in the transition state were found to be 1.55 Å for peroxy O—H bond and 1.01 Å for C—O—H bond. Evidently the hydrogen atom of the peroxide molecule is closer to the carbonyl oxygen atom than peroxy oxygen, corroborating the above statement.

In both cases, we propose that the first TST is similar; the difference is the proton source, which is a strong acid in the catalyzed case, and can be a proton water or hydrogen peroxyl atom in the uncatalyzed case. The protonation with strong acid is faster and more effective than with other proton sources because the strong acid proton has higher activity and reactivity than other hydrogen atoms; consequently, an increasing in the rate reaction is observed (about 10 times for a [H⁺] ~0.01 M).

4. Polymerization Step. Figures 2 and 7 show important Raman features that are very important and decisive in the elucidation of the proposed mechanism, among which are the following: splitting of the $\nu_{\text{s(C-C)}}$ and $\delta_{(\text{CH}_3)}$ bands of the acetone structure, which appear at 800 cm⁻¹ and 1420 cm⁻¹ in the Raman spectrum of acetone, and formation of new bands at 590 cm⁻¹ and 960 cm⁻¹ related to $\delta_{(\text{O-C-O})}$ and $\nu_{\text{a(C-O)}}$ vibration mode of the P1-monomer and TATP structure, respectively, which are indications of a change in the environment of the monomer unit structure as the polymerization progresses and generation of a single bond type. This is consistent with Scheme 2a-d.

The high similarity found in the Raman spectra of all the mixtures studied taken at different days, particularly in the fingerprint region of the spectra, is evidence that just the C—O bonds have been formed and the intermediaries have highly similar structures as proposed by the route above. In the mechanism proposed, the bonds formed are of the same type (C—O). Therefore, the Raman spectra of the polymeric structures designated as P₁, P₂, and P₃ should not differ significantly. In fact, the only variation observed was in the intensity and unfolding of some signals, which indicates growth of the polymer chain. In other words, the monomeric unit is changing its chemical environmental as the polymer chain increases in length.

To further corroborate the above statements, kinetic measurements were made, resulting in good agreement with the proposed mechanism. The formation of a new band corresponding to $\omega_{\text{O-C-O}}$ ²² that rapidly appeared around ~540 cm⁻¹ in the Raman shift spectrum and then decayed with a second order kinetics pattern is in complete agreement with the postulation of the dimerization stage (see Figure 7 and Scheme 2b).

The kinetic orders of the different decays were corroborated with the fractional time method. This method is based on the average values obtained for the quotient of $t_{3/4}/t_{1/2}$ ²³ in which values of 2 and 3 are confirmatory for first and second order, respectively. The average values found for the kinetics fittings shown in Figures 3 and 7 were 1.99 and 2.99, respectively, at several points of the decaying intensities, corroborating the key kinetics orders for the proposed mechanism (see Table 1). The C—O band decays with first order rate while the new band disappears after forming with second order rate kinetics. All kinetic decays were adjusted using the method of nonlinear

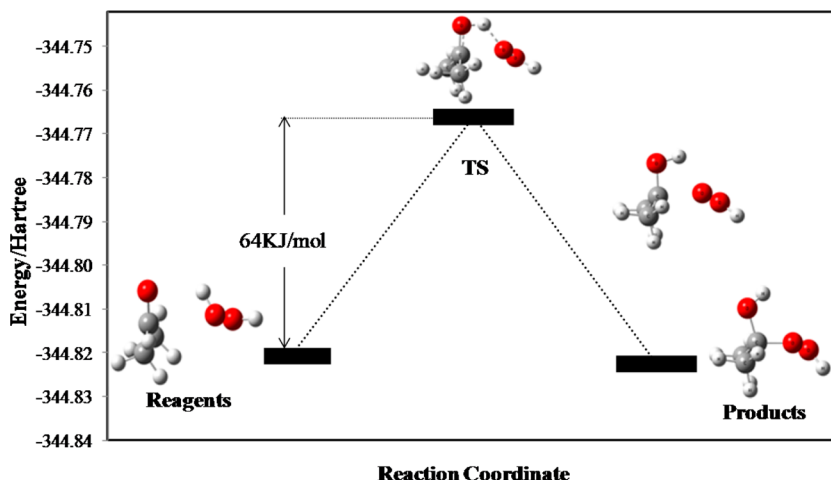


Figure 6. Energy diagram and sequence of atomic movements in the first step at DFT level. The atomic motion sequences were as follows: initial nucleophilic attack of lone electron pair of carbonyl oxygen atom of acetone to peroxide H atom; formation of a new O–H bond and decrease of C=O bond order; quick interaction between the peroxy oxygen atom and the carbonyl carbon atom; finally, formation of new C–O bond.

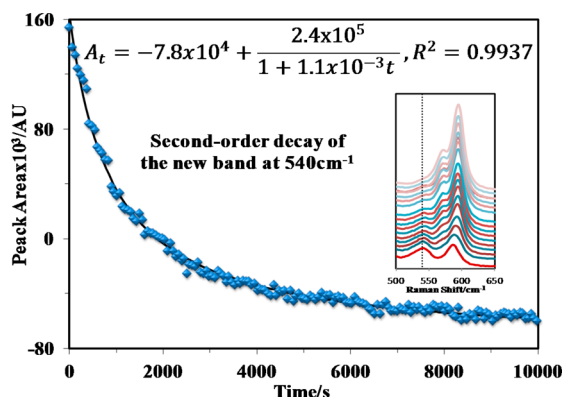


Figure 7. Second-order decay of the new band at 495 cm^{-1} for an uncatalyzed reaction.

Table 1. Fractional Times for Different Kinetics Orders and Quotient of Fractional Times for Acetone and New Band Decaying

order	$t_{3/4}/t_{1/2}$ predicted value	$t_{3/4}/t_{1/2}$ value for decaying of carbonyl band	$t_{3/4}/t_{1/2}$ value for decaying for new band formed
0	1.5	1.8	3.0
1	2.0	2.2	2.9
2	3.0	2.0	3.0

least-squares, which adjusted well to the respective kinetic behavior, as reflected in R^2 value. The average value of constant k_1 (first step) is lower than the average value for k_2 (dimerization reaction) by about 30–70 times; therefore, the second reaction is much faster than first one. Another interesting finding is that the

activation energy or energetic barrier of the first step is twice as high as the polymerization step, which reaffirms the results previously reported by Torent'ev et al, that the polymerization reaction is more energy favored than keto-peroxy reactions.¹² On the other hand, the experimental activation energies (E_a) were consistent with theoretical calculations in terms of trend. Table 2 summarizes all kinetics constants and activation energies at the temperature range studied. The kinetics pattern equations in terms of physical measurements for first and second order were adapted from Espenson.²³

5. Theoretical Support of the HPC Steps. The polymerization and cyclization steps were proposed to occur through an HPC reaction based on the charge densities on the hydroxyl and peroxy oxygen atoms, which are higher and sterically favorable on hydroxyl oxygen atom than the peroxy oxygen. Figure 8 shows a cross section of the molecular electrostatic potential distribution (MEP) of the O–C–O–O plane of the P₁ monomer structure. The red and yellow lines represent the electronegative potential and electropositive potential, respectively. This picture clearly shows that the hydroxyl oxygen atom has electronegative potential lines more pronounced and extended than peroxy oxygen atoms by covering a higher electronegative area. In other words, the electron cloud of hydroxyl oxygen is mostly delocalized, by converting it in a point more suitable for an electrophilic attack or an interaction with proton atom. Relevant computational values for Mulliken charge densities of hydroxyl oxygen atoms and peroxy oxygen atoms calculated at DFT level of theory using B3LYP hybrid functional and 6-311g++(d, p)^{18–20} basis set are contained in Table 3. A comparison to the natural bond orbital scheme (NBO) was done showing consistent data. The HPC reaction also is supported by the results of Terent'ev et al, which affirms that peroxy-alkoxy

Table 2. Constant Rate and Activation Energy for All Possible Reaction, Calculated at DFT Level Using B3LYP Hybrid Functional and 6-311g++(d, p) Basis Set

T/K	k_1	k_2	E_{a1} (KJ/mol)		E_{a2} (KJ/mol)	
			Exp.	DFT	Exp.	DFT
303.15	$(8.4 \pm 0.4) \times 10^{-4}$	$(567 \pm 17) \times 10^{-4}$				
313.15	$(15 \pm 2) \times 10^{-4}$	$(670 \pm 17) \times 10^{-4}$				
323.15	$(24 \pm 7) \times 10^{-4}$	$(825 \pm 16) \times 10^{-4}$				
333.15	$(37 \pm 3) \times 10^{-4}$	$(1188 \pm 16) \times 10^{-4}$				
			41 ± 5	64	21 ± 3	29

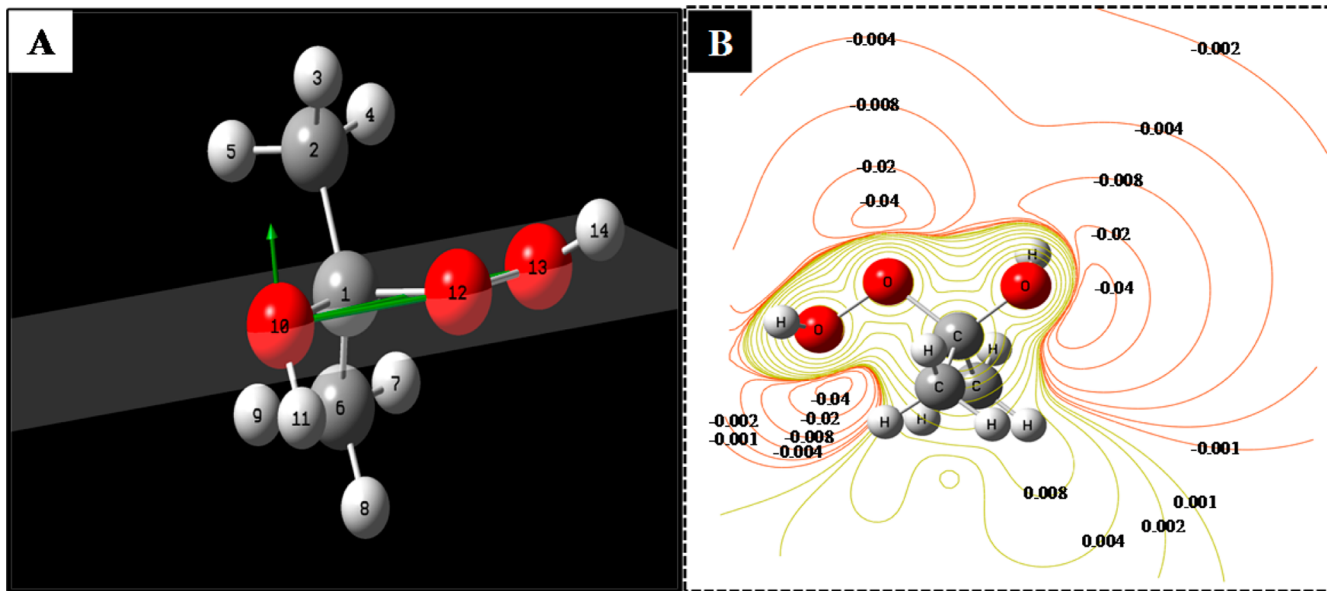


Figure 8. (a) O–O–C–O reference plane on which, the charge distribution was sketched. (b) Molecular electrostatic potential (MEP) contour map of the O–O–C–O plane: A cross section of the electrostatic spatial distribution at DFT level and B3LYP/6-311++g(d, p) basis set. The red lines represent the negative potential and the yellow lines positive potential.

Table 3. Mulliken Atomic and NBO Charges of Hydroperoxy and Alkoxy Oxygen Atoms of the Terminal Groups Calculated at DFT Level Using B3LYP Hybrid Functional and 6-311g++(d,p) Basis Set^a

atom	charge density					
	P ₃		P ₂		P ₁	
	Mulliken	NBO	Mulliken	NBO	Mulliken	NBO
terminal hydroxyl oxygen atom	-0.7536	-0.6250	-0.6570	-0.6250	-0.6605	-0.6260
terminal peroxide	-0.5102	-0.3250	-0.3533	-0.3260	-0.3750	-0.3130
oxygen atoms	-0.3646	-0.3990	-0.3243	-0.4000	-0.3316	-0.4090

^aP₁, P₂, and P₃ are polymeric structures.

condensation reaction is more energetically favorable than a keto-peroxy condensation reaction.¹² On the other hand, several researchers have reported some of the intermediate structures proposed in this manuscript.^{8,9,13,14}

6. Cyclization Step and Total Kinetic. The kinetics patterns of the global and some individual steps were measured through intensity decays of the key Raman active vibrations and were successfully related to the proposed mechanism. The global kinetics was expressed in terms of TATP (see detail in Supporting Information), and this concentration was monitored using $\nu_{\text{a}(\text{C}-\text{O})}$ band, which appears at 940 cm⁻¹ and is an important nonoverlapping band of this compound. The appearance of TATP was corroborated with GC measurements of solution standard; clearly, the formation of water is instantaneous (see chromatogram in the Supporting Information). The TATP formation does not take thirty days as is reported;^{1,16} what is delayed is the precipitation of crystals from reaction media.

Although all HPC-reactions have similar energy barriers, in a polymerization reaction, the more probable collisions are expected to occur between monomer (P₁) and long-polymer (P_n) molecules, or it is possible that the pre-exponential factor (A) of the Arrhenius law is higher than in other possible encounters, because the monomer molecule has greater diffusion power than other long chain-polymers. Consequently, the polymeric chain is elongated by progressive addition of monomer molecules.²⁴ Another important experimental fact is that TATP is the cyclic product of higher proportion in a catalyzed and

uncatalyzed AP-reaction (over 90% purity);^{1,13–16} therefore, other cyclization reactions are not significant in the overall kinetic when compared to cyclization of P₃ polymer. Taking into account the above physical consideration and experimental facts revealed a total kinetic expression in function of TATP concentration that successfully correlates with the temporal decay of the Raman intensity of the TATP nonoverlapping band with high R² acceptance value. Although the kinetic total equation showed a decaying term (e^{-kt}), this term is preceded by a minus sign that converts it into an increasing term ($-e^{-kt}$) (see eq 1).

$$[\text{TATP}]_t = \frac{1}{2k_8} [\text{AP}]_0 - \frac{1}{2k_8} [\text{AP}]_0 e^{-2k_1 t} \quad (1)$$

In this equation, [AP] is the concentration of the acetone-peroxide complex; k₁ and k₈ are the constant rates that lead from the monomer and TATP formation, respectively.

This important result demonstrates that the postulated mechanism is a viable route for the TATP formation uncatalyzed reaction (see Figure 9). The mathematical details of the kinetic law derivation are included as Supporting Information. On the other hand, we propose that the acid-catalyzed CAP reaction follows a mechanistic route analogous to that proposed here with some differences in terms of energy. In fact, as a corroborating result, the total kinetic of the TATP formation in a catalyzed reaction follows the same pattern as that of the uncatalyzed one (see Figure 10). At high acid concentrations, the AP-reaction

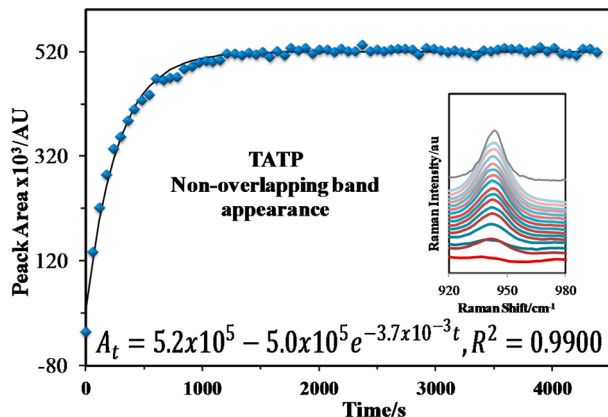


Figure 9. Kinetic decay of the TATP nonoverlapping band at 940 cm^{-1} for the uncatalyzed reaction.

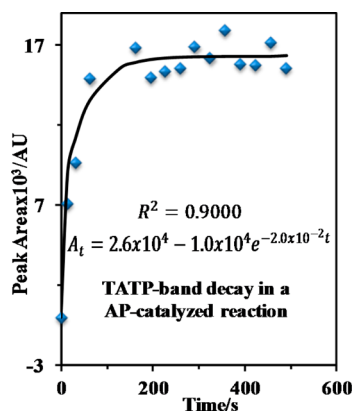


Figure 10. Kinetic decay of the TATP nonoverlapping band at 940 cm^{-1} for the acid-catalyzed reaction. The acid concentration was $1 \times 10^{-3}\text{ M}$ of H_2SO_4 .

releases a lot of energy, which leads to reactions of higher energetic requirement. Sometimes, this reaction becomes so energetically uncontrollable that it causes loud explosions. The remarkable increase in the reaction rate of the acid-catalyzed CAP reaction is due to the alkoxy ending that is readily protonated by the acid-catalyst, which is a stronger acid than water or hydrogen peroxide, releasing a water molecule faster than uncatalyzed reaction, generating more reactive intermediates and giving rise to an infinite number of reactions. This assessment explains the presence of several intermediaries such as diperroxyl structures proposed in CAP-mechanisms previously published.^{8,9,13–15}

7. Evidence of Some Intermediate Structures. Nuclear magnetic resonance (NMR) measurements are in agreement with the suggested intermediate structures proposed in the mechanism. NMR chemical shifts obtained are summarized in Table 4. ^1H NMR shifts at 4.5–5 ppm and 3–4 ppm correspond to the peroxy and hydroxyl proton, respectively. In order to

distinguish between them, a ^1H NMR spectra in deuterium oxide was obtained, and it was found that the ^1H NMR shift at 3–4 ppm is related to hydroxyl proton, since the peroxy proton is less exchangeable than the hydroxyl one. On the other hand, consistent results in ^1H NMR and ^{13}C NMR shifts were found in relation to the proposed polymeric structures P_1 , P_2 , and P_3 . For each type of carbon atom, one signal was observed, confirming that there are three different monomer environments in high proportion compared to other possible polymer structures. The third ^{13}C NMR shift at 100–110 ppm was not observed because either the abundance of ^{13}C isotope (1.1%) is too low for its detection or some of them have the same shift. This does not occur with the ^1H NMR spectra, due to the fact that ^1H abundance is much higher (about 99.8%).²⁵ Another possible cause related to not being able to detect the third ^{13}C NMR shift is that once the three units polymer (P_3) is formed, cyclization occurs to form TATP.

In order to corroborate some structural identities of the proposed mechanistic route and to consider it as a viable pathway of CAP-reaction leading to TATP, DADP, and other cyclic products, a GC-MS study was done on the reaction mixture, effectively confirming the presence of P_1 and P_2 intermediaries. Figures 11–12 show the electron impact MS spectra of these intermediates. In these, the molecular ions of 92 m/z and 166 m/z , which are the molecular weights of these structures, respectively, can be identified readily. Another important result is that both MS spectra presented the same fragmentation pattern; additionally, P_2 MS spectrum showed a fragment at 91 m/z , which is related to the 2-hydroperoxy-2-propan-2-ol moieties; the low intensity of respective MS-fragments is due to the electron impact sensitivity and thermal instability of these organic peroxide compounds, even after optimizing the GC-MS conditions to reduce thermal breakdown.^{26,27}

8. Test of the CAP Mechanism with *t*-Alcohols. The mechanism of the TATP formation reaction is proposed to be successive alkoxy-peroxy condensation reactions, in which the intermediary molecules have both alkoxy and peroxy terminal groups to keep forward the reaction progress analogous to a condensation polymerization process. If species with hydroxyl tails such as *tert*-alcohols are added to the CAP-reaction mixture, these molecules could react with the peroxy tail of the intermediary molecules, stopping the reaction progress and consequently inhibiting the TATP formation, given that alkoxy-peroxy and *tert*-alkoxy-peroxy condensation reaction have comparable activation energies. This reaction is sketched in Scheme 4. The competitive inhibition is because products formed would not have terminal groups to continue the TATP formation process. A temporal profile of the $\nu_{\text{C=O}}$ band of the Raman spectrum shows how the concentration of acetone declines rapidly until TATP formation is completed in a normal CAP catalyzed reaction (see Figure 13a), while the Figure 13b shows how the concentration of acetone in a CAP-catalyzed reaction remains constant; when an amount of *t*-alcohol is added, it is evident that the reaction is stopped. Strictly, we can say that up to

Table 4. ^1H NMR and ^{13}C NMR Shifts of the Reaction Mixture in D_2O and Acetone- d_6 Deuterated Solvent

atom type	^1H NMR shift/ppm (observed signals)	^{13}C NMR shift/ppm (observed signals)
hydroxyl hydrogen	(HO)-C(CH ₃) ₂ -(OOH)	3.6 (1)
peroxy hydrogen	(HO)-C(CH ₃) ₂ -(OOH)	4.5 (1)
acetals carbon	(HO)-C(CH ₃) ₂ -(OOH)	----
methyl hydrogen	(HO)-C(CH ₃) ₂ -(OOH)	1.3–1.5 (3)
methyl carbon	(HO)-C(CH ₃) ₂ -(OOH)	----

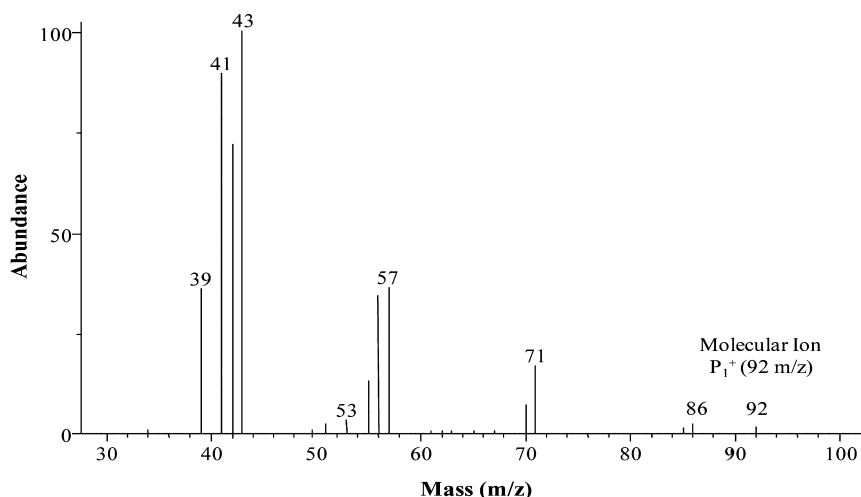


Figure 11. Electron impact MS spectrum of P_1 structure; monomer of the proposed mechanism. Molecular weight of this structure is 92 g/mol.

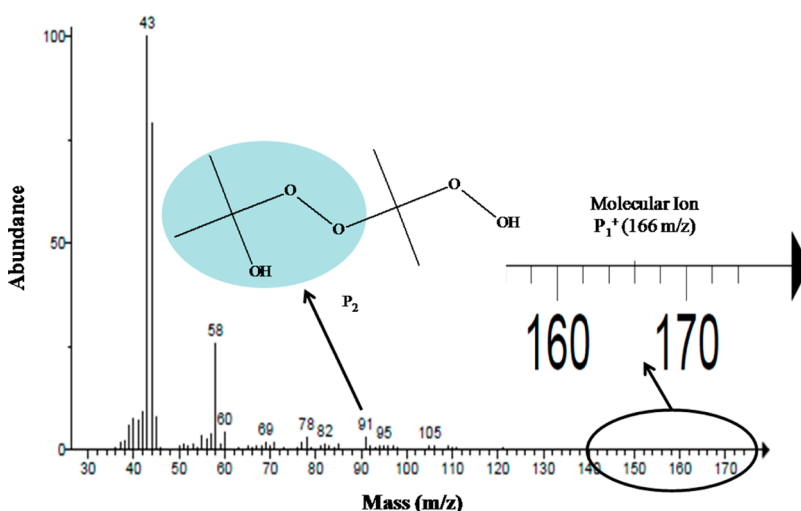
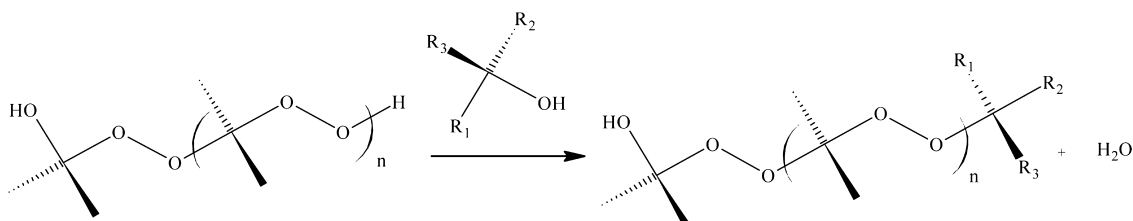


Figure 12. GC-EI MS of the gas phase AP formation reaction. The two main peaks at 0.86 and 2.20 min are related to acetone and P_2 , respectively.

Scheme 4. Competitive Inhibition Reaction of AP Formation with *tert*-Alcohols, These Compounds Clearly Stop AP-Formation



$t = 800$ s, the polymerization competes with the inhibition process, given that they are isoenergetic reactions; although the uninhibited case showed a minimal decreasing trend. Also, the inset photography after several days shows how inhibition of TATP is conserved. On the other hand, the acid-catalyzed reaction was studied at low concentrations of acid in order to appreciate significant results, given that the AP-acid catalyzed reaction is highly violent.

The inhibition reaction is said to be competitive, because the expected amounts of TATP formed is proportional to the amount of *tert*-alcohol added. Figure 14 shows in detail how the precipitation of TATP goes according to proportions of

tert-alcohol (1 to 5 servings of 260 μ L at 10.4 M) until the TATP formation is null at 1:1 molar ratio of acetone and *tert*-butanol. In detail, for each 1 mL of acetone at 13.7 M (\sim 0.00137 mol) were added progressively 1–5 servings of 260 μ L of *t*-alcohol at 10.4 M. The specific vibrational bands show evidence related to the $(R)_3C-O(H)$ bond shifting. Specifically, Figure 15 shows evidence of this chemical change. The O–H vibrational band (ν_{O-H}) of *t*-alcohol was not used to follow the competitive inhibition reaction, given that the reaction is carried out in aqueous media and is interfered by the O–H band of the water molecule. The chemical assay was done in two different

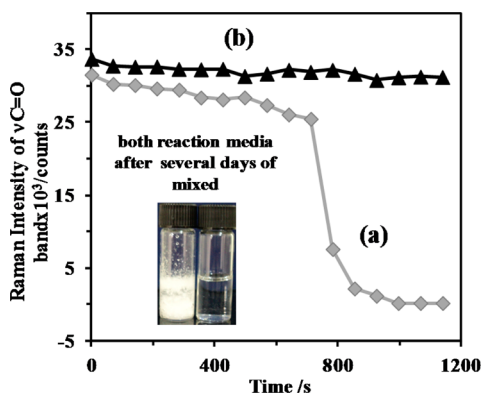


Figure 13. (a) Temporal decay of $\nu_{\text{C=O}}$ band of the Raman spectra in an AP acid catalyzed reaction; (b) decay of $\nu_{\text{C=O}}$ band in an AP-reaction when *t*-alcohol is added.

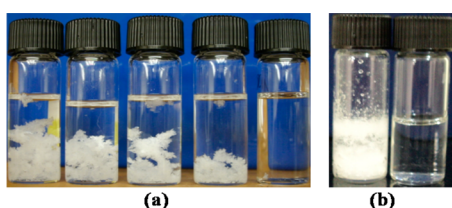


Figure 14. (a) Visual view of acetone-peroxide: *t*-butyl alcohol reaction at 5:1, 4:1, 3:1, 2:1, and 1:1 *t*-butyl alcohol:acetone ratio. The precipitated TATP is proportional to alcohol amount. (b) Acid catalyzed AP-reaction and AP-reaction plus T-alcohol.

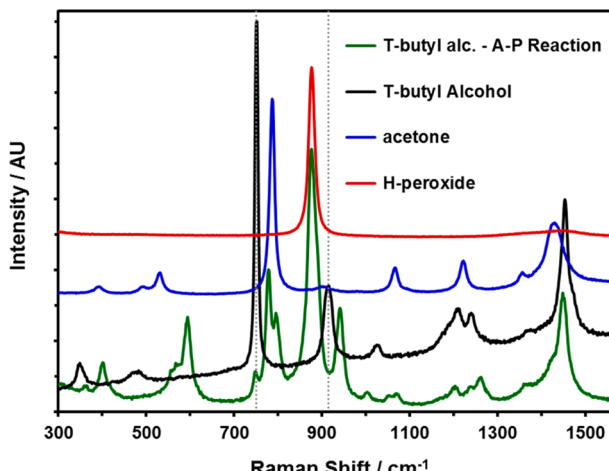


Figure 15. Acetone, *t*-butyl alcohol, and acetone-peroxide-*t*-butyl alcohol mix Raman spectra, the disappearing of $(\text{R})_3\text{C}-\text{OH}$ band is clearly observed, at 900 cm^{-1} . The spectra were followed using a 532 nm laser line.

tert-alcohols in order to corroborate this statement, by yielding the same results.

IV. CONCLUSION

It was possible to propose a viable mechanism for the cyclic acetone-peroxide reaction supported by Raman and NMR measurements and by theoretical calculations. The three independent approaches agree with each other with high consistency. The qualitative and quantitative Raman results confirm some key parts of the proposed mechanism, such as the experimental kinetics pattern and its respective kinetics order.

Splitting of Raman vibrations indicates the polymer growth in acetone-peroxide reactions. Independent measurements of ^1H NMR and ^{13}C NMR and GC-MS were used to corroborate some intermediate structures in the reaction media such as P_1 , P_2 , and P_3 , which are the precursors of the cyclic products.

ASSOCIATED CONTENT

S Supporting Information

Kinetic decays at several temperatures and its respective constants. Calculation of the activation energies. Mathematical deduction of the kinetic total based on TATP concentration. This material is available free of charge via the Internet at <http://pubs.acs.org>.

AUTHOR INFORMATION

Corresponding Author

*E-mail: rvivasr@unicartagena.edu.co.

Notes

The authors declare no competing financial interest.

ACKNOWLEDGMENTS

Support from the U.S. Department of Homeland Security under Award Number 2008-ST-061-ED0001 is also acknowledged. However, the views and conclusions contained in this document are those of the authors and should not be interpreted as necessarily representing the official policies, either expressed or implied, of the U.S. Department of Homeland Security. This contribution was also supported by the U.S. Department of Defense, Proposal Number: 58949-PH-REP, Agreement Number: W911NF-11-1-0152. The authors also acknowledge contributions from Dr. Richard T. Hammond from Army Research Office, DOD.

REFERENCES

- Wolffenstein, R. Ueber die Einwirkung von Wasserstoffstofferoxyd auf Aceton und Mesityloxyd. *Ber. Dtsch. Chem. Ges.* **1985**, *28*, 2265–2269.
- Evans, H. K.; Tulleners, F. A. J.; Sanchez, B. L.; Rasmussen, C. A. An Unusual Explosive, Triacetonetriperoxide (TATP). *J. Forensic Sci.* **1986**, *31*, 1190–1125.
- White, G. M. An Explosive Drug Case. *J. Forensic Sci.* **1992**, *37*, 652–656.
- Yinon, J.; Zitrin, S. Modern Methods and Applications in Analysis of Explosives; Wiley: Chichester, 1993; pp 305.
- Dubnikova, F.; Kosloff, R.; Almog, J.; Zeiri, Y.; Boese, R.; Itzhaky, H.; Alt, A.; Keinan, E. Decomposition of Triacetone Triperoxide is an Entropic Explosion. *J. Am. Chem. Soc.* **2005**, *127*, 1146–1159.
- Bellamy, A. J. Triacetone Triperoxide: Its Chemical Destruction. *J. Forensic Sci.* **1999**, *44*, 603–609.
- Hiyoshi, R. I.; Nakamura, J.; Brill, T. B. Thermal Decomposition of Organic Peroxides TATP and HMTD by T-Jump/FTIR Spectroscopy. *Propellants Explos. Pyrotech.* **2007**, *32*, 127–134.
- Oxley, J. C.; Smith, J. L.; Steinkamp, L.; Zhang, G. Factors Influencing Triacetone Triperoxide (TATP) and Diacetone Diperoxide (DADP) Formation: Part 2. *Propellants Explos. Pyrotech.* **2013**, *38*, 1–11.
- Oxley, J. C.; Smith, J. L.; Bowden, P. R.; Rettinger, R. C. Factors Influencing Triacetone Triperoxide (TATP) and Diacetone Diperoxide (DADP) Formation: Part I. *Propellants Explos. Pyrotech.* **2013**, *38*, 244–254.
- Jensen, L. P.; Mortensen, M.; Trane, R.; Harris, P.; Berg, R. W. Reaction Kinetics of Acetone Peroxide Formation and Structure Investigations using Raman Spectroscopy and X-ray Diffraction. *Appl. Spectrosc.* **2008**, *63*, 92–97.

- (11) Armitt, D.; Zimmermann, P.; Ellis, S. Gas Chromatography/Mass Spectrometry Analysis of Triacetone Triperoxide (TATP) Degradation Products. *Rapid Commun. Mass Spectrom.* **2008**, *22*, 950–958.
- (12) Torent'ev, A. O.; Platonov, M. M.; Sonneveld, E. J.; Peschar, R.; Chernyshev, V. V.; Starikova, Z. A.; Nikishin, G. I. New Preparation of 1,2,4,5,7,8-Hexaoxonanes. *J. Org. Chem.* **2007**, *72*, 7237–7243.
- (13) Sauer, M. C. V.; Edwards, J. O. The Reactions of Acetone Hydrogen Peroxide. I. Higher Adducts. *J. Phys. Chem.* **1972**, *76*, 1283–1288.
- (14) Sauer, M. C. V.; Edwards, J. O. The Reactions of Acetone Hydrogen Peroxide. I. Primary Adducts. *J. Phys. Chem.* **1971**, *75*, 3004–3011.
- (15) Story, P. R.; Lee, B.; Bishop, C. E.; Denson, D. D.; Busch, P. Macrocyclic Synthesis. II. Cyclohexanone Peroxides. *J. Org. Chem.* **1970**, *35*, 3059–3062.
- (16) Milas, N.; Golubovic, A. Studies in Organic Peroxides. XXVI. Organic Peroxides Derived from Acetone and Hydrogen Peroxide. *J. Am. Chem. Soc.* **1959**, *81*, 6461–6462.
- (17) Fukui, K. The Path of Chemical Reactions – The IRC approach. *Acc. Chem. Res.* **1981**, *14*, 363–368.
- (18) Becke, A. D. Density-functional Thermochemistry III. The Role of Exact Exchange. *J. Chem. Phys.* **1993**, *98*, 5648–5649.
- (19) Lee, C.; Yang, W.; Parr, R. G. Development of the Colle-Salvetti Correlation-Energy Formula into a Functional of the Electron Density. *Phys. Rev.* **1988**, *B37*, 785–789.
- (20) Hehre, W. J.; Radom, L.; Schleyer, P. V. R.; Pople, J. A. *Ab Initio Molecular Orbital Theory*; Wiley: New York, 1986.
- (21) Frisch, M.; Schlegel, H.; Scuseria, G.; Robb, M.; Cheeseman, J.; Montgomery, J.; Vreven, T.; Kudin, K.; Burant, J.; Millam, J. et al. *Gaussian 03W*, revision B.04; Gaussian, Inc., Pittsburgh, PA, 2003.
- (22) Sigman, M. E.; Clark, C. D.; Caiano, T.; Mullen, R. Analysis of Triacetone Triperoxide (TATP) and TATP Synthetic Intermediates by Electrospray Ionization Mass Spectrometry. *Rapid Commun. Mass Spectrom.* **2008**, *22*, 84–90.
- (23) Espenson, J. H. *Chemical Kinetics and Reaction Mechanisms*; Speer, J., Morris, J. M., Eds.; Series in Advanced Chemistry; McGraw-Hill Inc.: New York, 1995; pp 32.
- (24) Sutthasupa, S.; Shiotsuki, M.; Sanda, F. Recent Advances in Ring-Opening Metathesis Polymerization, and Application to Synthesis of Functional Materials. *Polym. J.* **2010**, *42*, 905–915.
- (25) Paudler, W. W. *Nuclear Magnetic Resonance*; Bush, D. H., Shull, H., Eds.; Allyn and Bacon Chemistry Series; University of Alabama: Boston, 1971; pp 17–32, 220–237.
- (26) Espinosa-Fuentes, E. A.; Pacheco-Londoño, L. C.; Barreto-Cabán, M. A.; Hernández-Rivera, S. P. Novel Uncatalyzed Synthesis and Characterization of Diacetone Diperoxide. *Propellants Explos. Pyrotech.* **2012**, *37*, 413–421.
- (27) Pacheco-Londoño, L. C.; Pena-Quevedo, A. J.; Primera-Pedrozo, O. M.; Hernández-Rivera, S. P.; Mina-Camilde, N.; García, R.; Chamberlain, R. T.; Lareau, R. T. *Proc. SPIE* **2004**, *5403*, 279–287.